Engineering Perspective 5 (2): 49-59, 2025

e-ISSN:2757-9077

ENGINEERING PERSPECTIVE

https://sciperspective.com

Research Paper

View Factor Calculations Between Triangular Surfaces

Yanan Camaraza-Medina[1*], Abel Hernandez-Guerrero[1], Jose L. Luviano-Ortiz[1]

[1]*Department of Mechanical Engineering, University of Guanajuato, Guanajuato, Mexico*

ABSTRACT

In radiative heat transfer calculations, to determine the view factor between surfaces is crucial. Currently, the available technical literature on the subject lacks an analytical expression for estimating the view factor for combinations of triangular surfaces. An analytical solution requires the summation of multiple integrals, given the changes in the integration contours, which becomes more complex in irregular contours. This work aims to develop an expression for computing the view factor between 32 triangular geometric configurations with a common edge and included angle θ. Very importantly, in modern engineering, mesh generators rarely use rectangles or squares (unless the overall geometry is a perfect cube), with triangular elements being the most commonly used elements. For comparison, 48 cases with diverse geometric relationships were calculated using the analytical solution (AS), numerical integration using Simpson's multiple 1/3 rule (MSR), the Sauer graphical solution (SGS), and Bretzhtsov cross roots (BCR). From eight basic geometries, the view factor was computed for the remaining 24 combinations using the sum rule. In all cases, identical fit values were obtained for MSR and SGS with respect to AS, while BCR showed the best correlation in all cases examined. In all the cases evaluated, the BCR showed the best fits, with an error of ±6% in more than 90% of the sample s, while the MSR showed an average dispersion of ±6% in 65% of the data. Given the practical nature of the contribution and the reasonable values of the fits obtained, the current proposal constitutes a suitable tool for application in thermal engineering.

Keywords: Bretzhtsov cross roots; Radiative heat transfer; Triangular surfaces; View factor

History
Received: 15.03.2025
Revised : 23.04.2025
Accepted: 14.05.2025

Author Contacts: ycamaraza1980@yahoo.com, abel@ugto.mx, luis.luviano@ugto.mx

Cite this paper: Camaraza-Medina, Y., Hernadez-Guerrero, A., Luviano-Ortiz, J. L. (2025). View factor calculation between triangular surfaces. Engineering Perspective, 5 (2), 49-59. http://dx.doi.org/10.29228/eng.pers.81688

*Corresponding Author

1. Introduction

In many engineering applications, radiative heat transfer between surfaces needs to be assessed. The view factor allows calculating the fraction of radiant energy emitted by one surface that reaches another. Therefore, the geometric relationship between two surfaces and its influence on the view factor has been the subject of research for decades. In previous work, various analytical and numerical solutions have been proposed for different configurations [1-5]. An expanded collection of view factors for over 340 different configurations is provided by Howell [6].

Several methods are known in the literature for estimating view factors, including graphical, analytical, and visual methods. Furthermore, using the summation rule and the algebraic factor, view factors of already known geometries can be used to determine other view factors of derived or more complex geometries [7-10].

The current increase in data processing in computational techniques has enabled the use of commercial programs based on the Finite Element Method (FEM) to solve various heat transfer problems, including thermal radiation. Solutions for edge and border problems generally reduce to surfaces with a common edge and included angle θ, for which analytical solutions are already known [11-15]. However, in modern engineering, mesh generators rarely use rectangles or squares (unless the overall geometry is a perfect cube), with triangular elements being the most commonly used.

The AS of the view factor between triangular geometries requires the summation of multiple integrals, given the changes in the integration contours, which makes it difficult to obtain solutions in complex configurations. Numerical integration can be a partial solution to the problem; however, only a few contributions to the topic are available in the specialized literature [16].

By numerical integration using the RMS and five intervals, the view factors for various triangular geometries with a common edge and an angle $\theta = 90^{\circ}$ were obtained. The results for the most elementary ones were graphed and the remaining geometries derived using the summation rule [17]. SGS are useful, but they require the interpretation of graphs, which introduces reading and interpretation errors. Therefore, they are not suitable for generating triangular meshes and subsequently calculating view factors, as they lack an analytical solution or a numerical approximation for their estimation.

The BCR is a mathematical tool that allows for obtaining reasonable fits in the approximations of complex functionals, in addition to generating an analytical expression that includes the boundary conditions or unknowns to be addressed. Therefore, it can be used to calculate view factors without the need to use or interpret graphs. The method in question allows for fitting by sections or branches, with common nodes for several solutions [18, 19]. Its mathematical conception is similar to that of the FEM, making it suitable for this work.

Currently, there is no analytical expression in the specialized literature that allows directly calculating the view factor for combinations of triangular surfaces. In the expanded compilation of view factor configurations available for the case of finite triangular surfaces, it is verified that only Sauer's graphical results are used [6]. In other consulted sources, Sauer graphs are also presented for the determination of view factors [18, 20]. The above shows that currently there are no exact or approximate analytical solutions for the determination of view factors between triangular geometries with a common edge and included angle θ, which is the main objective of this work.

Therefore, this research aims to develop approximate solutions that allow computing the view factor in various triangular geometries. These solutions do not present high mathematical complexity and their correlation with respect to the AS provides a better fit than the SGS. This constitutes a new analytical method for application to the calculation of view factors using FEM and to constituting new expressions that can be included in existing catalogs.

In this work, the exact analytical solutions for eight basic triangular geometries and their respective Bretzhtsov cross roots are given. For comparison, 48 examples with various aspect ratios were calculated for each geometry, using the AS, the numerical solution of the quadruple integral using the MSR with five intervals, the SGS and the view factors calculated using the BCR. From the eight basic geometries, the view factor for another 24 triangular geometries is obtained using the summation rule. In all cases, identical fit values were obtained for RMS and SGS with respect to AS, while BCR showed the best fit in all cases examined, confirming the validity of the hypothesis regarding its use.

Given the practical nature of the contribution and the reasonable values of the fits obtained, the proposal presented in this work constitutes a suitable tool for application in thermal engineering and related practices that require thermal radiation calculations.

2. Materials and methods

2.1 Basic considerations on the view factor

The view factor is fundamental to the exchange of radiant energy. It depends on the configuration and position of the receiving and emitting surfaces, making its evaluation complex and, in many cases, generating erroneous results. Then, the view factor F_{12} is the fraction of the radiation emitted by surface A_1 that is intercepted by surface A_2, expressed as [21]:

$$F_{12} = \frac{1}{\pi A_1} \int_{A_1}^{A_2} \int_{A_2}^{A_1} \frac{\cos\theta_1 \cos\theta_2}{r^2} \, dA_1 \, dA_2 \tag{1}$$

where A_1, A_2 are the emitting and receiving surfaces, respectively; θ_1, θ_2 are the angles between the normal vector to the area $dA_1 dA_2$ and the line joining the centers of surfaces A_1, A_2, respectively; r is the distance between the centers of surfaces A_1 and A_2 (see Figure 1).

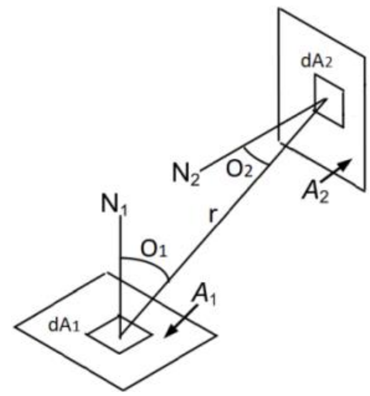

Figure 1. Basic geometry for view factor definition

Eq. (1) includes double integration, which in many cases can be a very laborious mathematical problem. Therefore, calculating the view factor in any geometry requires handling a considerable amount of integrals and solving complex mathematical equations. To simplify the analysis, numerical approximations are used that provide adequate fits, with a reasonable margin of error, allowing for its application in practical engineering. For three-dimensional configurations, several methods can be implemented to estimate the view factor, such as direct integration, contour integration, summation and reciprocity techniques, MSR, Monte Carlo, ray tracing, FEM, and matrix methods [22-28].

In this investigation, the direct integration method was implemented to obtain the view factors associated with the 32 configurations studied. The BCR method was used to approximate the special functions generated in direct integration.

2.2 Mathematical solution for the view factor

The view factor between two finite rectangles of the same width with a common edge and included angle θ (see Figure 2) is given by:

$$f_{(1)} = \frac{\sin^2\theta}{\pi A_1} \int_0^L dy_1 \int_0^D dx \int_0^W dz \int_0^D \frac{xz}{\{(y_1-y_2)^2 + x^2 + z^2 - 2xz\cos\theta\}^2} dy_2 \tag{2}$$

To evaluate Eq. (2) the following definitions are used:

$$X = W/D \quad ; \quad Y = L/D \quad ; \quad R = \sqrt{X^2 + Y^2 - 2XY\cos\theta} \tag{3}$$

$$f_{(1)}=\mathrm{F}_{\mathrm{a-b}}=\frac{1}{\pi \mathrm{Y}}\left\{\begin{array}{c}-\frac{\sin 2\theta}{4}\left\{Y^2\tan^{-1}\left(\frac{X}{Y}\csc\theta-\cot\theta\right)+X^2\tan^{-1}\left(\frac{Y}{X}\csc\theta-\cot\theta\right)+XY\sin\theta+\left(\frac{\pi}{2}-\theta\right)(X^2+Y^2)\right\}+\\ +\frac{1}{4}\ln\left\{\left\{\frac{X^2}{R^2}\left(\frac{1+X^2}{1+R^2}\right)^{\cos 2\theta}\right\}^{X^2\sin^2\theta}\left(\frac{Y^2+Y^2R^2}{R^2+Y^2R^2}\right)^{Y^2\sin^2\theta}\left(\frac{(1+X^2)(1+Y^2)}{1+R^2}\right)^{\cos^2\theta+1}\right\}+\\ +(\sin^3\theta\cos\theta)\tan^{-1}\left(\frac{Y\sin\theta\sqrt{X^2+\cot^2\theta+1}}{X^2-YX\cos\theta+1}\right)\sqrt{X^4+X^2(\cot^2\theta+1)}++X\tan^{-1}\left(\frac{1}{X}\right)+\\ +Y\tan^{-1}\left(\frac{1}{Y}\right)+-R\cot^{-1}(R)+\frac{\sin 2\theta}{2}\int_0^Y\sqrt{z^2+\cot^2\theta+1}\tan^{-1}\left(\frac{X\sin\theta\sqrt{z^2+\cot^2\theta+1}}{z^2-zX\cos\theta+1}\right)dz\end{array}\right\} \quad (4)$$

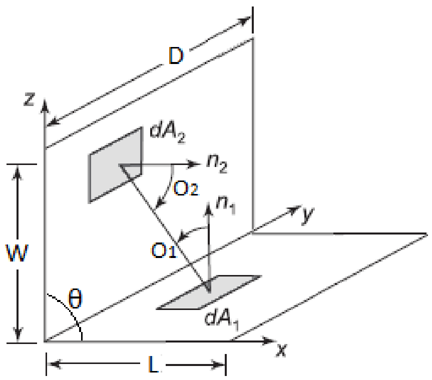

Figure 2. Rectangles with common edge and included angle θ

Evaluating Eq. (2), the following solution is obtained [29]:

In Eq. (2) and (4) the angle θ is given in radians. In a previous investigation [30], an expression similar to Equation (4) was obtained to solve the quadruple integral given in Eq. (2), tabulating the values of the viewing factors for the angles θ = (30°; 45°; 60°; 90°; 120°; 135°; 150°). These valueswere later corrected because they sometimes violated the summation rule [31-33].

Eq. (4) is very complex. The last integral lacks primitives, so it was not possible to solve it. Therefore, its solution will be obtained using the MSR (with eight intervals). At each interval of the numerical integration, the variable z is replaced by its corresponding fraction of the length of the emitting surface L (see Table 1), obtaining a solution (ω_n) for each interval [29].

Table 1. Definition of z-scores for the MSR in Eq. (4).

0	Int. 1	Int. 2	Int. 3	Int. 4	Int. 5	Int. 6	Int. 7	Int. 8
0	$0.125L$	$0.25L$	$0.375L$	$0.5L$	$0.625L$	$0.75L$	$0.875L$	L
ω_1	ω_2	ω_3	ω_4	ω_5	ω_6	ω_7	ω_8	ω_9

Therefore, the numerical evaluation of the last integral given in Eq. (4) can be calculated as:

$$\int_0^Y\left\{\sqrt{1+z^2\sin^2\theta}\tan^{-1}\left(\frac{X\sqrt{1+z^2\sin^2\theta}}{z^2-zX\cos\theta+1}\right)\right\}dz\cong\frac{L}{24}(\omega_1+\omega_9+2(\omega_3+\omega_5+\omega_7)+4(\omega_2+\omega_4+\omega_6+\omega_8)) \quad (5)$$

If $\theta=90^{\circ}$, then Eq. (4) simplifies to the following relation:

$$f_{(1)}=\frac{1}{\pi Y}\left\{X\tan^{-1}\left(\frac{1}{X}\right)+Y\tan^{-1}\left(\frac{1}{Y}\right)-R\cot^{-1}(R)+\frac{1}{4}\ln\left\{\left(\frac{X^2+X^2R^2}{R^2+X^2R^2}\right)^{X^2}\left(\frac{Y^2+Y^2R^2}{R^2+Y^2R^2}\right)^{Y^2}\left(\frac{(1+X^2)(1+Y^2)}{1+R^2}\right)\right\}\right\} \quad (6)$$

In Eq. (6), the following definitions are used:

$$X=W/D \quad ; \quad Y=L/D \quad ; \quad R=\sqrt{X^2+Y^2} \quad (7)$$

Figure 3 shows graphically the solutions to Eq. (4) for values of $\theta=(30^{\circ},45^{\circ},60^{\circ},90^{\circ},120^{\circ},150^{\circ})$, in the intervals $0.1\le Y;X\le 10$. For angle values $\theta\ne(30^{\circ},45^{\circ},60^{\circ},90^{\circ},120^{\circ},150^{\circ})$, the view factor can be obtained by interpolation.

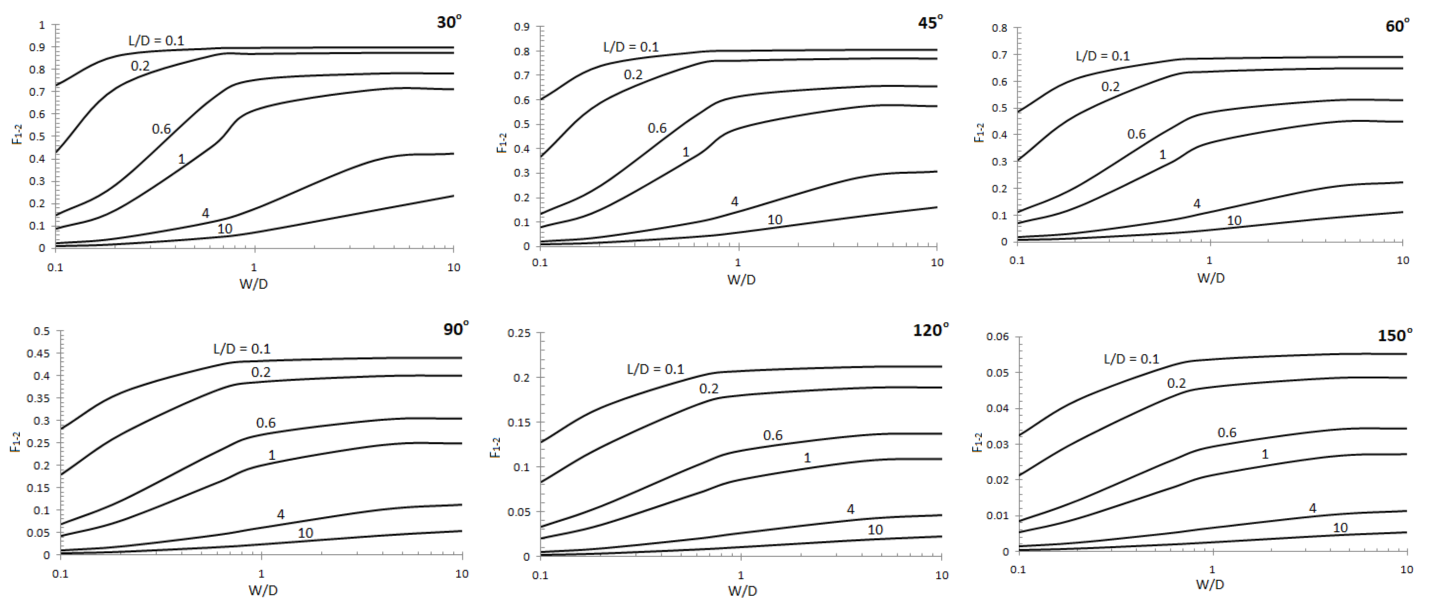

Figure 3. $\mathrm{F}_{\mathrm{a-b}}$ values obtained with Eq. (4) for various values of θ.

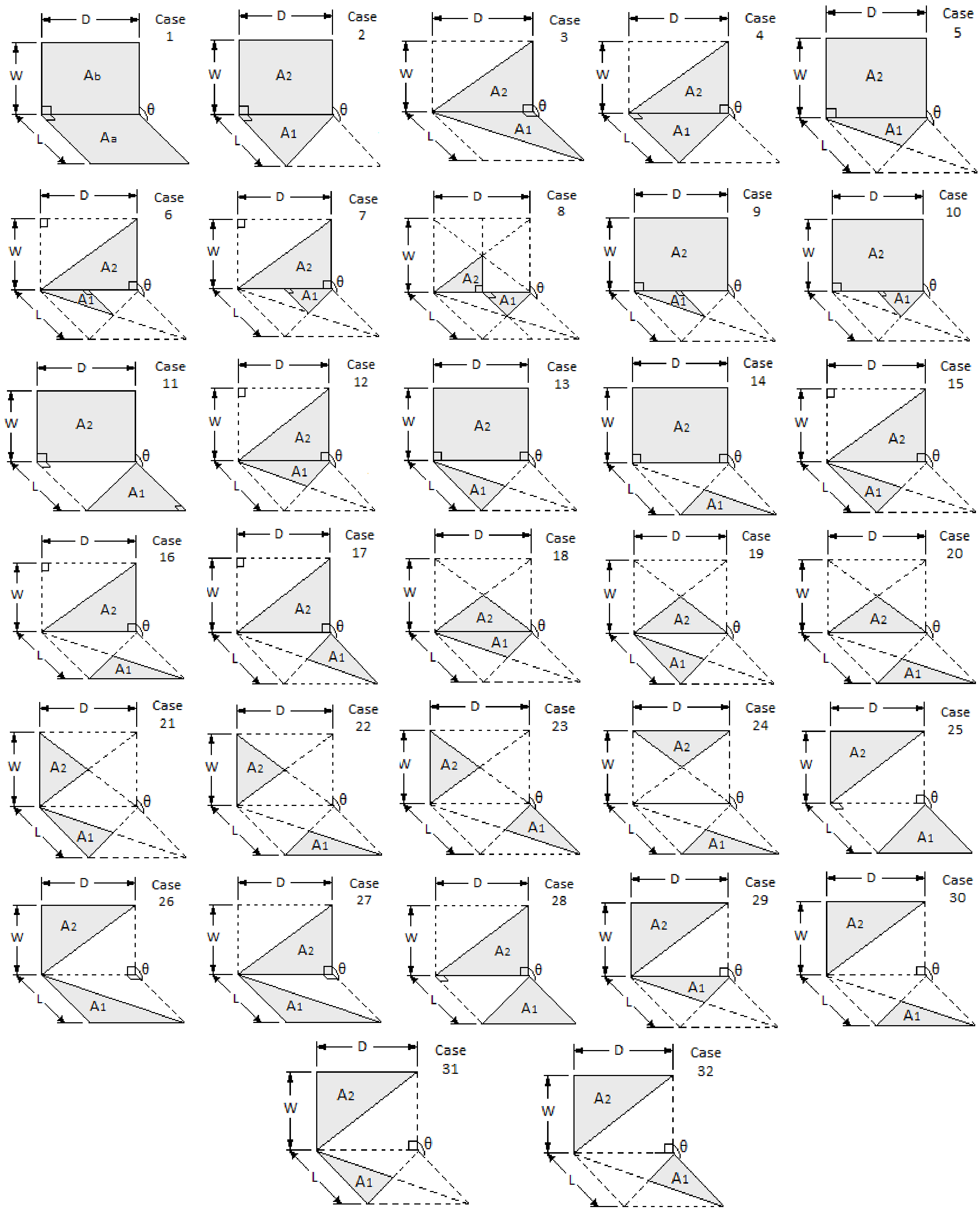

Figure 4. Basic configurations for triangular surfaces

2.3 Mathematical solution for the view factor

In modern engineering, mesh generators rarely use rectangles or squares, unless the overall geometry is a perfect cube. One of the most commonly used elements is triangular ones. The formulation of this type of geometry requires a mathematical approach that includes multiple sums of the quadruple integral. due to the variation of the projection contours on the coordinate axes. Diagonal lines can be extended over the rectangular surfaces in Figure 2, subdividing the rectangular plane domain into triangular elements (see Figure 4).

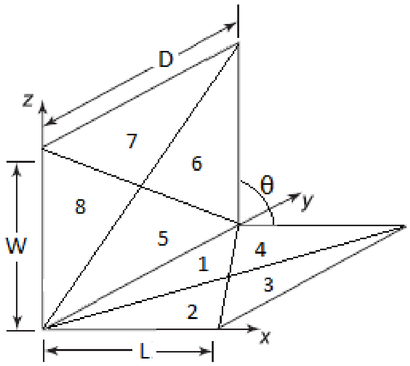

Figure 5. Decomposition of triangular elements

In Figure 5, the leaving and reaching surfaces A_a and A_b are divided into four triangular surfaces, with 64 possible combinations. The reciprocity of the viewing factors establishes that $A_aF_{a-b} = A_bF_{b-a}$; therefore, only 32 combinations will be evaluated. The basic geometries (Cases 1 to 8) and derived geometries (Cases 9 to 32) are given in Figure 4. The basic geometries (Cases 1 to 8) constitute the basis of the study conducted, as the remaining combinations can be generated from them using the summation rule.

2.4 Mathematical modeling of the view factor

2.4.1 Case 2

In Case 2, the emitting and receiving surfaces are a rectangle and a right triangle, respectively, with common side D and angle θ between both surfaces. In Case 2 (see Figure 6), the integration limits are set for each projection on surfaces A_1 and A_2, obtaining the following relation:

$$f_{(2)} = \frac{\sin^2\theta}{\pi A_1}\int_0^L dy_1 \int_0^{\frac{y_1 D}{L}} dx \int_0^W dz \int_0^D \frac{xz}{\{(y_1-y_2)^2+x^2+z^2-2xz\cos\theta\}^2}\,dy_2 \tag{8}$$

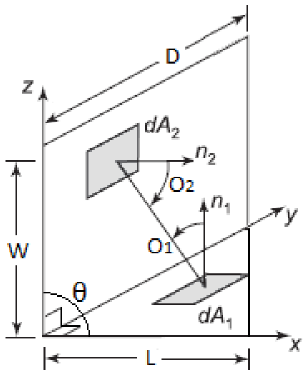

Figure 6. Basic Geometry for Case 2

The solution of Eq. (8) is given by:

$$\begin{aligned} f_{(2)} = 2f_{(1)}\Bigg\{ & \frac{X^2}{2(X^2+1)^2}\ln\left\{\left(\frac{1}{X}\right)^{2X^2}\left(\frac{X^2+Y^2}{Y^2+1}\right)\left(\frac{1}{X(X^2+Y^2)}\right)^{(X^2+1)}\right\} + \frac{1}{4}X^2\ln\left\{\left(\frac{X^6}{(X^2+1)^2}\right)\left(\frac{X^2+Y^2+1}{X^2+Y^2}\right)\right\} - -\sqrt{X^2+Y^2}\tan^{-1}\left(\frac{1}{\sqrt{X^2+Y^2}}\right) + \\ & \frac{1}{4}\ln\left\{(X^2+1)\left(\frac{Y^2+1}{X^2+Y^2+1}\right)\right\} + \frac{1}{4}Y^2\ln\left\{\frac{Y^4(X^2+Y^2+1)}{(Y^2+1)(X^2+Y^2)^2}\right\} + Y\tan^{-1}\left(\frac{1}{Y}\right) + + \frac{(X^2+1)(X^4+3X^2)+2X\pi\left(X^2-\frac{1}{2}(3X^2+1)\right)}{4(X^2+1)^2} + \\ & \frac{X^3\left(\frac{1}{X^2+1}-Y^2-1\right)}{(X^2+1)^{\frac{3}{2}}\sqrt{X^2Y^2-\frac{X^2}{X^2+1}+X^2}}\tan^{-1}\left(\frac{X(X^2+1)^{\frac{3}{2}}\sqrt{X^2Y^2-\frac{X^2}{X^2+1}+X^2}}{(X^2+1)\left(X^2Y^2-\frac{X^2}{X^2+1}+X^2\right)-X^4}\right) + + \frac{3}{2}X\tan^{-1}\left(\frac{1}{X}\right) + \frac{X^2}{4(X^2+1)}\ln\left\{\frac{Y^2+1}{(X^2+Y^2)X^2}\right\} + \frac{X^2Y^2}{4(X^2+1)}\ln\left\{\frac{X^2+2Y^2+1}{Y^2(X^2+Y^2)} + \right. \\ & \left. 1\right\} - -\frac{1}{X}\int_0^X\left\{\frac{z^2}{\sqrt{z^2+Y^2}}\tan^{-1}\left(\frac{\sqrt{z^2+Y^2}}{\frac{1}{X^2}(z^2-Xz)+z^2+Y^2}\right) + \frac{z}{\sqrt{z^2+Y^2}}\tan^{-1}\left(\frac{\frac{z}{X}-1}{\sqrt{z^2+Y^2}}\right)\right\}dz\Bigg\} \end{aligned} \tag{9}$$

In Eq. (9) the term $f_{(1)}$ is the view factor computed with Eq. (4). Solving Eq. (8) requires solving $n^n = 4^4 = 256$ primitive functions. However, the last integral was not solved because no primitive functions existed for it, requiring a solution using the MSR (with seven intervals). Obtaining an analytical solution to Eq. (8) is extremely complex, as it involves the summation of infinite series with polylogarithms. An alternative solution is to treat these special functions as complex variables, with the addition of polynomials, which progressively tend toward convergence of the infinite Spence series, using BCR. Case 2 was obtained from the decomposition of rectangular surfaces into triangular elements (see Figure 4); therefore, the solution to the quadruple integral of Eq. (8) is derived from Eq. (4) and can be expressed as:

$$F_{1-2} = \varphi \cdot f_{(1)} \tag{10}$$

where $f_{(1)}$ is the view factor computed with Equation (4) and φ is the BCR.

The BCR is obtained from a stationary sum of view factors, fitting the family of curves generated in the evaluated domain using polynomials. There will be as many curves to fit as terms considered in the sum of the series of polylogarithms; therefore, the increase in the intervals will be proportional to the accuracy obtained in the results. In Equation (4), it is observed that the view factor depends on two parameters X, Y with a common denominator D; therefore, the real root will be a function of these. The common side D is opposite to the dimensions W, L on the surfaces A_a and A_b, which indicates that the period of the complex function is given by [18]:

$$\psi = \tan^{-1}(X/Y) \tag{11}$$

To apply the BCR, the solution to Eq. (10) is graphically represented in the interval $0.1 \leq X \leq 10$ and $0.1 \leq Y \leq 10$ using values $X = Y = (0.1;\ 0.3;\ 0.6;\ 1;\ 3;\ 6;\ 10)$ for its construction. Therefore, from the upper and lower nodes, it is possible to draw the curve corresponding to the minimum and maximum values of $Y = (0.1\ ;10)$. In the infinite polylogarithmic series, a value of Y is fixed, and subsequently the polylogarithms are calculated for each value of X; with this procedure, a family of curves a is obtained. Next, a similar procedure is applied, but fixing the values of X when calculating the polylogarithms for each value of Y, thus obtaining a family of curves b. Curves a and b are approximated individually using the least squares method, generating polynomials of the form $mX^3 + nX^2 + oX + p$. The constants m, n, o, p are subsequently weighted to generate a single function φ, which depends on the forming angle ψ [19]. Applying the method described in the previous paragraph, the BCR for Case 2 is given by:

$$\varphi_2 = (-0{,}022\mathrm{Y}^3 + 0{,}316\mathrm{Y}^2 - 0{,}89\mathrm{Y} + 0{,}5)\psi^2 + (0{,}056\mathrm{Y}^3 - 0{,}783\mathrm{Y}^2 + 2{,}23\mathrm{Y} - 1{,}43)\psi - 0{,}03\mathrm{Y}^3 + 0{,}407\mathrm{Y}^2 - 1{,}07\mathrm{Y} + 2{,}02 \quad (12)$$

Substituting Eq. (4) and (12) in Eq. (11), the view factor for Case 2 is obtained through the BCR, which is given by the following relation:

$$f_{(2)} = F_{(1-2)} = \varphi_2 \cdot f_{(1)} \quad (13)$$

Figure 7 presents graphically the solution of Eq. (13) for $\theta = 90°$.

Cases 3 to 8 are reduced to the following geometries:

Case 3: right triangle to right triangle, with a common side and angle θ between both surfaces: vertices at a common point

Case 4: right triangle to right triangle, with a common side and angle θ between both surfaces: vertices at opposite ends

Case 5: isosceles triangle to right triangle, with a common side and angle θ between both surfaces

Case 6: right triangle to right triangle of different sizes, with angle θ between both surfaces: vertices at a common point

Case 7: right triangle to right triangle of different sizes, with angle θ between both surfaces: vertices at opposite ends

Case 8: perpendicular right triangles with an equal edge and arranged in opposite directions.

In Cases 3 to 8 (see Figure 5), the integration limits are established for each projection on surfaces A_1 and A_2, obtaining the following integral relations:

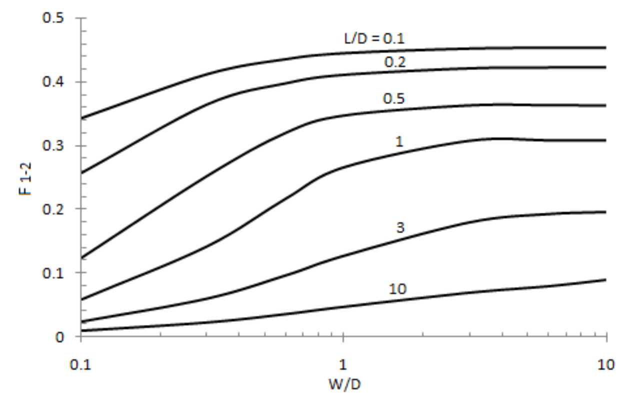

Figure 7. Graphical solution of Eq. (13) for $\theta = 90°$

2.4.2 Cases 3 to 8

Case 3 $$f_{(3)} = \frac{1}{\pi A_1}\iint \frac{\cos O_1 \cos O_2\, dA_1 dA_2}{r^2} = \frac{\sin^2\theta}{\pi A_1}\int_0^L dy_1 \int_0^{y_1 D/L} dx \int_0^W dy_2 \int_0^{y_2 D/W} \frac{xz}{\{(y_1-y_2)^2+x^2+z^2-2xz\cos\theta\}^2} dz \quad (14)$$

Case 4 $$f_{(4)} = \frac{1}{\pi A_1}\iint \frac{\cos O_1 \cos O_2\, dA_1 dA_2}{r^2} = \frac{\sin^2\theta}{\pi A_1}\int_0^L dy_1 \int_0^{y_1 D/L} dx \int_0^W dy_2 \int_0^{y_2 D/W} \frac{xz}{\{(y_1-y_2)^2+x^2+z^2-2xz\cos\theta\}^2} dz \quad (15)$$

Case 5 $$f_{(5)} = \frac{1}{\pi A_1}\iint \frac{\cos O_1 \cos O_2\, dA_1 dA_2}{r^2} = \frac{\sin^2\theta}{\pi A_1}\int_0^{L/2} dy_1 \int_0^{y_1 D/L} dx \int_0^W dz \int_0^Z \frac{xz}{\{(y_1-y_2)^2+x^2+z^2-2xz\cos\theta\}^2} dy_2 \quad (16)$$

Case 6 $$f_{(6)} = \frac{1}{\pi A_1}\iint \frac{\cos O_1 \cos O_2\, dA_1 dA_2}{r^2} = \frac{\sin^2\theta}{\pi A_1}\int_0^{L/2} dy_1 \int_0^{y_1 D/L} dx \int_0^W dy_2 \int_0^{y_2 D/W} \frac{xz}{\{(y_1-y_2)^2+x^2+z^2-2xz\cos\theta\}^2} dz \quad (17)$$

Case 7 $$f_{(7)} = \frac{1}{\pi A_1}\iint \frac{\cos O_1 \cos O_2\, dA_1 dA_2}{r^2} = \frac{\sin^2\theta}{\pi A_1}\int_0^{L/2} dy_1 \int_{-y_1 D/L}^{0} dx \int_0^W dy_2 \int_0^{y_2 D/W} \frac{xz}{\{(y_1-y_2)^2+x^2+z^2-2xz\cos\theta\}^2} dz \quad (18)$$

Case 8 $$f_{(8)} = \frac{1}{\pi A_1}\iint \frac{\cos O_1 \cos O_2\, dA_1 dA_2}{r^2} = \frac{\sin^2\theta}{\pi A_1}\int_0^{L/2} dy_1 \int_{-y_1 D/L}^{0} dx \int_0^{W/2} dy_2 \int_0^{y_2 D/W} \frac{xz}{\{(y_1-y_2)^2+x^2+z^2-2xz\cos\theta\}^2} dz \quad (19)$$

The BCR for each case are given by:

Case 3 $$f_{(3)} = f_{(1)} \cdot \{(-0{,}001\mathrm{Y}^3 + 0{,}033\mathrm{Y}^2 - 0{,}14\mathrm{Y} + 0{,}265)\psi^2 + (0{,}011\mathrm{Y}^3 - 0{,}177\mathrm{Y}^2 + 0{,}7\mathrm{Y} - 0{,}615)\psi - 0{,}01\mathrm{Y}^3 + 0{,}142\mathrm{Y}^2 - 0{,}475\mathrm{Y} + 1{,}29\} \quad (20)$$

Case 4 $$f_{(4)} = f_{(1)} \cdot \{(-0{,}031\mathrm{Y}^3 + 0{,}424\mathrm{Y}^2 - 1{,}275\mathrm{Y} + 1{,}1)\psi^2 + (0{,}071\mathrm{Y}^3 - 0{,}975\mathrm{Y}^2 + 2{,}92\mathrm{Y} - 2{,}06)\psi - 0{,}034\mathrm{Y}^3 + 0{,}462\mathrm{Y}^2 - 1{,}268\mathrm{Y} + 1{,}6\} \quad (21)$$

Case 5 $$f_{(5)} = f_{(1)} \cdot \{(-0{,}01\mathrm{Y}^2 + 0{,}24\mathrm{Y} + 0{,}67)\psi^2 + (0{,}02\mathrm{Y}^2 - 0{,}31\mathrm{Y} - 2{,}2)\psi - 0{,}02\mathrm{Y}^2 + 0{,}27\mathrm{Y} + 3\} \quad (22)$$

Case 6 $$f_{(6)} = f_{(1)} \cdot \{(-0{,}02Y^3 + 0{,}29Y^2 - 1{,}1Y + 0{,}6)\psi^2 + (0{,}06Y^3 - 0{,}88Y^2 + 2{,}96Y - 1{,}41)\psi - 0{,}04Y^3 + 0{,}55Y^2 + 1{,}41Y + 1{,}87\} \quad (23)$$

Case 7 $$f_{(7)} = f_{(1)} \cdot \{(-0{,}011Y^3 + 0{,}12Y^2 - 0{,}025Y + 0{,}52)\psi^2 + (0{,}025Y^3 - 0{,}307Y^2 + 0{,}49Y - 1{,}64)\psi - 0{,}014Y^3 + 0{,}183Y^2 - 0{,}35Y + 2{,}47\} \quad (24)$$

Case 8 $$f_{(8)} = f_{(1)} \cdot \{(0{,}015Y^2 - 0{,}108Y + 0{,}08)\psi^2 + (-0{,}015Y^2 + 0{,}096Y + 0{,}048)\psi - 0{,}001Y^2 + 0{,}04Y + 0{,}058\} \quad (25)$$

Figure 8 gives a graphical solution to Eq. (20) to (22), for $\theta = 90°$.

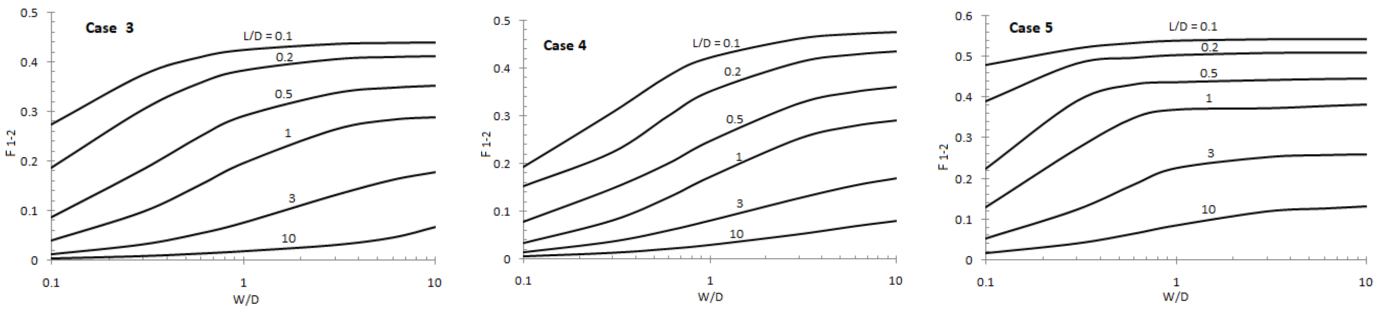

Figure 8 Graphical solutions of Equations (20) to (22) for $\theta = 90°$.

Figure 9 gives a graphical solution to Eq. (23) to (25), for $\theta = 90°$.

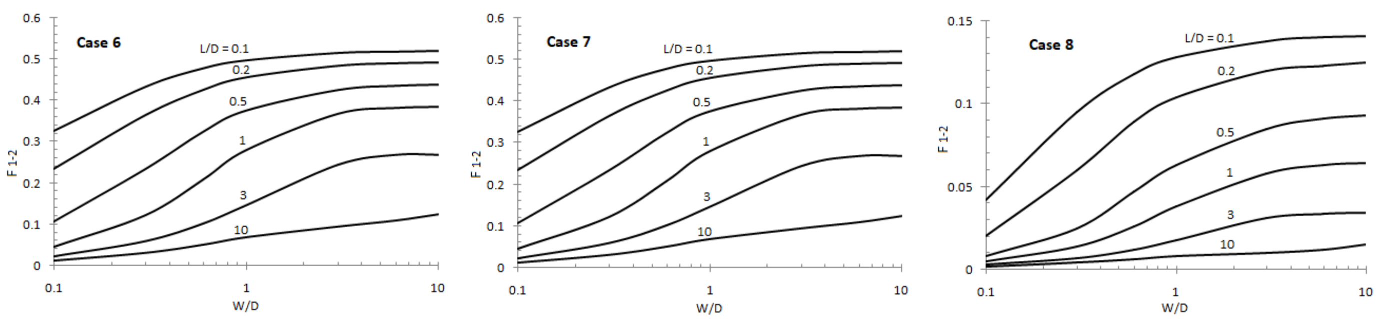

Figure 9 Graphical solutions of Equations (22) to (25) for $\theta = 90°$.

2.4.3 Cases 9 to 32

By combining the view factors $f_{(1)}$ to $f_{(8)}$ it is possible to obtain the view factors for Cases 9 to 32 by applying the summation rule and the algebra of view factors. Table 2 summarizes the relationships for computing the view factor in the derived configurations (see Figure 4).

3 Analysis of Results

The percentage of deviation (error) is calculated with respect to the AS and computed as follows:

$$D_{\%} = 100 \cdot \left(\frac{SA - Val}{SA}\right) \quad (26)$$

Where: $D_{\%}$ is the percentage of deviation, in %, AS is the view factor computed using the analytical solution, and Val is the view factor obtained using other methods.

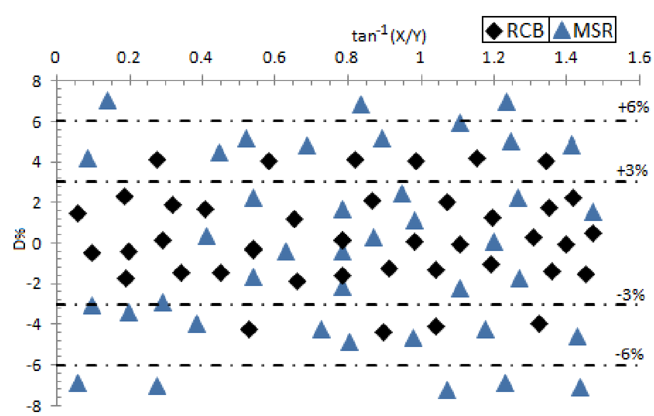

Figure 10. $D_{\%}$ values computed for Case 2

Figure 10 shows the $D_{\%}$ obtained with Eq. (26) for 42 view factors in the range $0.1 \le X, Y \le 10$ calculated with MSR and BCR for Case 2, plotted in error bands of ±3% and ±6%.

For Case 2, Figure 10 shows that the BCR provides a better fit with respect to the AS, with a mean error of ±3% and ±6% for 80.8% and 100% of the points (Y,X) analyzed. In contrast, the view factors obtained with MSR provide a weaker fit respect to the AS, with mean errors of ±3% and ±6% for 42.9% and 88.1% of the points (Y,X) evaluated, respectively.

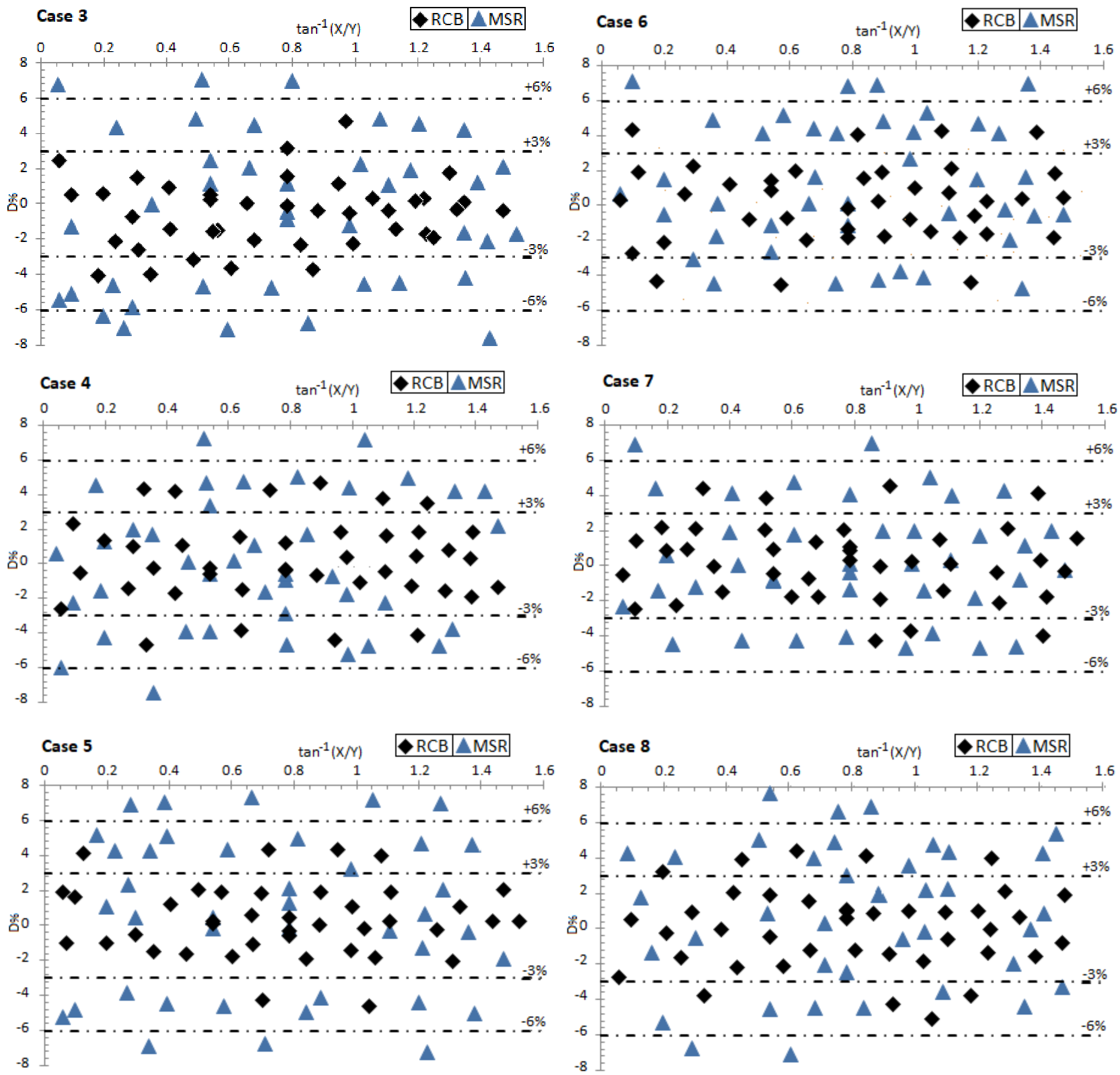

Figure 11. $D_{\%}$ values for Cases 3 to 8.

Figure 11 shows the $D_{\%}$ obtained using Eq. (26) for 42 view factors in the range $0.1 \leq X, Y \leq 10$, calculated using MSR and BCR for Cases 3 to 8, in error bands of ±3% and ±6%.

For Case 3, Figure 11 shows that the BCR provides the best fit with respect to the AS, with an average error of ±3% and ±6% in 85.7% and 100% of the points (Y,X) analyzed. In contrast, the view factors obtained using MSR produce a weaker fit with respect to the AS, with average errors of ±3% and ±6% in 45.2% and 81.1% of the points (Y, X) evaluated, respectively.

For Case 4, Figure 11 shows that the BCR provide a better fit than the AS, with mean errors of ±3% and ±6% in 76.2% and 100% of the points (Y,X) analyzed, while the view factors obtained with MSR provide a weaker fit with respect to the AS, computing mean errors of ±3% and ±6% in 47.6% and 90.5% of the points (Y,X) evaluated, respectively.

For Case 5, Figure 11 shows that the BCR provide a better fit with respect to the AS, with mean errors of ±3% and ±6% in 90.5% and 100% of the points (Y,X) analyzed. In contrast, the view factors obtained with MSR provide a weaker fit with respect to the AS, with mean errors of ±3% and ±6% in 50% and 78.6% of the points (Y,X) evaluated, respectively.

For Case 6, Figure 11 shows that the BCR provide a better fit with respect to the AS, with mean errors of ±3% and ±6% in 83.3% and 100% of the points (Y,X) analyzed, while the view factors obtained with MSR provide a weaker fit with respect to the AS, computing mean errors of ±3% and ±6% in 35.7% and 88.9% of the points (Y,X) evaluated, respectively.

For Case 7, Figure 11 shows that the BCR provide a better fit compared to the AS, with mean errors of ±3% and ±6% at 90.5% and 100% of the points (Y,X) analyzed. In contrast, the view factors obtained with MSR provide a weaker fit compared to the AS, with mean errors of ±3% and ±6% at 61.9% and 95.2% of the points (Y,X) evaluated, respectively.

For Case 8, Figure 11 shows that the BCR provide a better fit with respect to the AS, with mean errors of ±3% and ±6% in 76.2% and 100% of the points (Y,X) analyzed, while the view factors obtained with MSR provide a weaker fit with respect to the AS, computing mean errors of ±3% and ±6% in 40.5% and 81.1% of the points (Y,X) evaluated, respectively.

Table 2. View factor for Cases 9 to 32.

Case	$F_{1-2}\cdots\{f_{(n)}\}$
Case 9	$f_{(9)} = f_{(5)}$
Case 10	$f_{(10)} = f_{(5)}$
Case 11	$f_{(11)} = 2f_{(1)} - f_{(2)}$
Case 12	$f_{(12)} = f_{(6)} + f_{(7)}$
Case 13	$f_{(13)} = 2f_{(2)} - f_{(5)}$
Case 14	$f_{(14)} = 4f_{(1)} + f_{(5)} - 4f_{(2)}$
Case 15	$f_{(15)} = 2f_{(4)} - f_{(6)} - f_{(7)}$
Case 16	$f_{(16)} = 4f_{(1)} + f_{(6)} + f_{(7)} - 2f_{(3)} - 2f_{(4)}$
Case 17	$f_{(17)} = 2f_{(3)} - f_{(6)} - f_{(7)}$
Case 18	$f_{(18)} = f_{(3)} + f_{(8)}$
Case 19	$f_{(19)} = f_{(6)} + f_{(7)} - f_{(3)} - f_{(8)}$
Case 20	$f_{(20)} = 4f_{(5)} + f_{(3)} + f_{(8)} - 2f_{(6)} - 2f_{(7)}$
Case 21	$f_{(21)} = 3f_{(3)} + f_{(8)} - 2f_{(6)} - 2f_{(7)}$
Case 22	$f_{(22)} = 4f_{(1)} + 3f_{(6)} + 3f_{(7)} - 3f_{(3)} - 2f_{(4)} - 4f_{(5)} - f_{(8)}$
Case 23	$f_{(23)} = 4f_{(5)} + f_{(3)} + f_{(8)} - 2f_{(6)} - 2f_{(7)}$
Case 24	$f_{(24)} = 5f_{(3)} + 4f_{(4)} + 5f_{(5)} + f_{(8)} - 4f_{(1)} - 4f_{(2)} - 4f_{(6)} - 4f_{(7)}$
Case 25	$f_{(25)} = 2f_{(1)} + f_{(4)} - 2f_{(2)}$
Case 26	$f_{(26)} = 2f_{(1)} + f_{(3)} - 2f_{(2)}$
Case 27	$f_{(27)} = f_{(2)} - f_{(3)}$
Case 28	$f_{(28)} = f_{(2)} - f_{(4)}$
Case 29	$f_{(29)} = f_{(5)} - f_{(6)} - f_{(7)}$
Case 30	$f_{(30)} = 2f_{(3)} + 2f_{(4)} + f_{(5)} - 4f_{(2)} - f_{(6)} - f_{(7)}$
Case 31	$f_{(31)} = 2f_{(2)} + f_{(6)} + f_{(7)} - f_{(5)} - 2f_{(4)}$
Case 32	$f_{(32)} = 2f_{(2)} + +f_{(6)} + f_{(7)} - f_{(5)} - 2f_{(3)}$

4. Conclusions

Determining the view factor is one of the most important features during analysis of radiant energy exchange, since an analytical solution considerably facilitates the work of thermal engineers, allowing its rapid and accurate estimation. This work has provided insight into the development of methods for calculating the view factor during radiant energy exchange between 32 combinations of triangular geometries with a common edge.

Twelve examples with various aspect ratios were calculated for each geometry, using AS, MSR, SGS, and BCR. From the eight basic geometries, the view factor was obtained for 24 other triangular geometries using the summation rule. In all cases, identical fit values were obtained for MSR and SGS with respect to AS, while BCR showed the best correlation in all cases examined. In all the cases evaluated, the BCR showed the best fits, with an error of ±6% in more than 90% of the samples, while the MSR showed an average dispersion of ±6% in 65% of the data

Given the practical nature of the contribution and the reasonable values of the fits obtained, the proposal constitutes a suitable tool for application in thermal engineering and related practices requiring thermal radiation calculations.

Very importantly, in modern engineering, mesh generators rarely use rectangles or squares (unless the overall geometry is a perfect cube), with triangular elements being the most commonly used elements.

Given the lack of similar precedents in the literature, the proposed analytical solutions reinforce the scientific and practical value of this research and can be incorporated into the currently available catalogs for calculating the view factor.

Acknowledgment

The authors acknowledge the help provided by Dr. M. Zeki Yilmazouglu, from the Department of Mechanical Engineering, Gazi University, Turkey.

Nomenclature

a	Length of the surface A_1, m
A_1	Leaving surface, m^2
A_2	Reaching surface, m^2
D	Width of the surfaces A_1 and A_2, m
$D_{\%}$	percentage of deviation, defined in Eq. (26)
L	Length of the surface A_1, m
r	Distance between surfaces A_1 and A_2, m
R	Constant, defined in Eq. (3)
x	displacement at surface A_2, defined in Fig. 4
W	Length of the surface A_2, m
X	Constant, defined in Eq. (3)
Y	Constant, defined in Eq. (3)
θ	Angle between surfaces A_1 and A_2
θ_1	Angle between the normal and surface A_1
θ_2	Angle between the normal and surface A_2
φ	Bretzhtsov cross roots

Conflict of Interest Statement

The authors declare that there is no conflict of interest in the study.

CRediT Author Statement

Yanan Camaraza-Medina: Conceptualization, Data curation, Formal analysis, Investigation, Supervision, Validation, Writing-original draft, Writing - review & editing **Abel Hernandez-Guerrero:** Supervision, Validation, Writing - review & editing **Jose L Luviano-Ortiz:** Formal analysis, Writing - review & editing

References

1. Camaraza-Medina, Y. (2021). Methods for the determination of the heat transfer coefficient in air cooled condenser used at biomass power plants. International Journal of Heat and Technology, 39 (5), 1443-1450. https://doi.org/10.18280/ijht.390505
2. Nassar, Y. F. (2020). Analytical-numerical computation of view factor for several arrangements of two rectangular surfaces with non-common edge. International Journal of Heat and Mass Transfer, 159, 120130. https://doi.org/10.1016/j.ijheatmasstransfer.2020.120130
3. Howell, J. R., & Mengüç, M. P. (2011). Radiative transfer configuration factor catalog: A listing of relations for common geometries. Journal of Quantitative Spectroscopy and Radiative Transfer, 112, 910-912. https://doi.org/10.1016/j.jqsrt.2010.10.002
4. Modest, F. M., & Mazumder, S. (2021). Radiative heat transfer, 4th ed., Academic Press,
5. Camaraza-Medina, Y., Hernandez-Guerrero, A., & Luviano-Ortiz, J. L. (2022). Analytical view factor solution for radiant heat transfer between two arbitrary rectangular surfaces. Journal of Thermal Analysis and Calorimetry, 147 (24), 14999–15016. https://doi.org/10.1007/s10973-022-11646-4
6. Howell, J. R. (2023). A catalog of radiation heat transfer configuration factors. 7th ed., MIT Press.
7. Narayanaswamy, A. (2015). An analytic expression for radiation view factor between two arbitrarily oriented planar polygons. International Journal of Heat and Mass Transfer, 91, 841-847. https://doi.org/10.1016/j.ijheatmasstransfer.2015.07.131
8. Narayanaswamy, A., & Meyappan, P. (2015). An analytic expression for radiation view factors between two planar triangles with arbitrary orientations. Advances in Computational Heat Transfer, 6, 2015-2019 https://doi.org/10.1615/ICHMT.2015.IntSympAdvComputHeatTransf
9. Gupta, M. K., Bumtariya, K. J., Shukla, H. A., Patel, P., & Khan, Z. (2017). Methods for evaluation of radiation view factor: a review. *Material Today Proceeding*, 4 (2), 1236-1243. https://doi.org/10.1016/j.matpr.2017.01.143
10. Howell, J. R., Mengüç, J. P., Daun, K., & Siegel, R. (2020). Thermal Radiation Heat Transfer, 7thed., CRC Press.
11. Ehlert, J. R., & Smith, T. F. (1993). View factors for perpendicular and parallel rectangular plates. Journal of Thermophysics and Heat Transfer, 7 (1), 173-175. https://doi.org/10.2514/3.11587
12. Yi, X. J., Zhong, L. Y., Wang, T. B., Liu, W. X., Zhang, D. J., Yu, T. B., & Liu, N. H. (2019). Near-field radiative heat transfer between hyperbolic metasurfaces based on black phosphorus. The European Physical Journal B, 92, e217. https://doi.org/10.1140/epjb/e2019-100274-y
13. Zhou, Y., Duan, R., Zhu, X., Wu, J., Ma, J., Li, X., Wang, Q. (2020). An improved model to calculate radiative heat transfer in hot combustion gases. Combustion Theory and Modelling, 24 (5), 829-851. https://doi.org/10.1080/13647830.2020.1769866
14. Reddy, R. S., Arepally, D., & Datta, A. K. (2023). View factor computation and radiation energy analysis in baking oven with obstructions: Analytical and numerical method. Journal of Food Process Engineering, 46 (3), 4270. https://doi.org/10.1111/jfpe.14270
15. Dam, Q.T., Haidar, F., Mama, N., & Chennapalli1, S. J. (2024). Modeling and simulation of an In ternal Combustion Engine using Hydrogen: A MATLAB implementation approach. Engineering Perspective, 4 (3), 108-118. http://dx.doi.org/10.29228/eng.pers.76219
16. Krishnaprakas, C. K. (1997). View factor between inclined rectangles. Journal of Thermophysics and Heat Transfer, 11 (3), 480-481. https://doi.org/10.2514/2.6267
17. Sauer, H. J. (1974). Configuration factors for radiant energy interchange with triangular areas. ASHRAE Transactions, 80 (2), 268-279.
18. Camaraza-Medina, Y., Hernandez-Guerrero, A., & Luviano-Ortiz, J. L. (2023). View factor for radiative heat transfer calculations between triangular geometries with common edge. Journal of Thermal Analysis and Calorimetry, 148 (10), 4523–4539. https://doi.org/10.1007/s10973-023-11975-y
19. Camaraza-Medina, Y. (2023). Polynomial cross-roots application for the exchange of radiant energy between two triangular geometries. Ingenius, Revista de Ciencia y Tecnología, 30, 29-41. https://doi.org/10.17163/ings.n30.2023.03
20. Thyageswaran, S. (2022). Simpler view factor calculations for mutually perpendicular rectangles. Journal of Quantitative Spectroscopy and Radiative Transfer, 283, 108151. https://doi.org/10.1016/j.jqsrt.2022.108151
21. Boeke, W., & Wall, L. (1976). Radiative exchange factors in rectangular spaces for the determination of mean radiant temperatures. Building Services Engineer, 43, 244-253.
22. Cabeza-Lainez, J. (2023). A New Principle for Building Simulation of Radiative Heat Transfer in the Presence of Spherical Surfaces. Buildings, 13 (6), 1447. https://doi.org/10.3390/buildings13061447
23. Cabeza-Lainez, J. (2024). New Geometric Theorems Derived from Integral Equations Applied to Radiative Transfer in Spherical Sectors and Circular Segments. *Mathematics*, *12* (18), 2875. https://doi.org/10.3390/math12182875
24. Lakhi, M., & Safavinejad, A. (2021). Numerical investigation of combined force convective–radiative heat transfer in a horizontal channel with lattice Boltzmann method. Journal of Thermal Analysis and Calorimetry, 146, 1911-1922. https://doi.org/10.1007/s10973-020-10136-9
25. Gomez-Gil, A., & Cabeza-Lainez, J. (2024). Ferrer House at Rocafort, an Early Case of Brise-Soleil's Design for the Mediterranean Region in Valencia. *Designs*, *8* (5), 96. https://doi.org/10.3390/designs8050096
26. Sönmez, F. F., Ziar, H., Isabella, O., & Zeman, M. (2019). Fast and accurate ray-casting-based view factor estimation method for complex geometries. Solar Energy Materials and Solar Cells, 200, 109934. https://doi.org/10.1016/j.solmat.2019.109934
27. Biehs, S. A., Messina, R., Venkataram, P. S., Rodriguez, A. W., Cuevas, J. C., & Ben-Abdallah, P. (2021). Near-field radiative heat

transfer in many-body systems. Reviews of Modern Physics, 93 (2), 025009. https://doi.org/10.1103/RevModPhys.93.025009

28. Camaraza-Medina, Y., Hernandez-Guerrero, A., Luviano-Ortiz, J.L. (2024). Contour integration for the view factor calculation between two rectangular surfaces. Heat Transfer, 53 (1), 225-243. https://doi.org/10.1002/htj.22950
29. Camaraza-Medina, Y., Hernandez-Guerrero, A., Luviano-Ortiz, J.L. (2024). Contour integration for the exchange of radiant energy between diffuse rectangular geometries. Thermal Science and Engineering Progress, 47, 102289. https://doi.org/10.1016/j.tsep.2023.102289
30. Hamilton, D. C., & Morgan, M. R. (1952). Radiant-interchange configuration factors. NAAS TN 2836.
31. Feingold, A. (1966). Radiant-interchange configuration factors between various selected plane surfaces. Proceedings of the Royal Society of London, 292, 51-60. https://doi.org/10.1098/rspa.1966.0118
32. DeSutter, J., Tang, L., & Francoeur, M. (2019). A near-field radiative heat transfer device. Nature Nanotechnology, 14 (8), 751-755. https://doi.org/10.1038/s41565-019-0483-1
33. Yarahmadi, M., Robert Mahan, J., & McFall, K. (2020). Artificial neural networks in radiation heat transfer analysis. ASME Journal of Heat Transfer, 142 (9), 092801. https://doi.org/10.1115/1.4047052